CIVIL ENGINEERING JOURNAL

Article no. 3

THE CIVIL ENGINEERING JOURNAL 1-2024

AN ELASTOPLASTIC CONSTITUTIVE MODEL OF LUNAR SOIL SIMULANT CONSIDERING SHEAR DILATANCY AND SOFTENING CHARACTERISTICS

Yunli Li[1], Luqi Wang[1], Jiawei Li[1], and Wenping Wu[2]

1. *School of Civil Engineering and Architecture, Wuhan Institute of Technology, Wuhan 430074, China; liyunli@wit.edu.cn*
2. *School of Civil Engineering, Wuhan University, Wuhan 430072, China*

ABSTRACT

The study of the constitutive relationship of lunar soil is the key to a deep understanding of the mechanical properties of lunar soil. Previous models mostly focused on the strengthening behavior, while rarely reflected the post-peak softening and residual deformation stages during shear deformation. A new elastoplastic constitutive relation is derived with combining kinematic hardening model and initial shear stress, which effectively compensates for the shortcomings of existing constitutive models, and the validity of the model is verified by comparing with existed laboratory test results. The developed constitutive model not only effectively captures the shear dilatancy and softening characteristics of lunar soil simulant, but also only requires fewer parameters to be easily determined by simple initial loading curves from direct shear tests, Furthermore, the influences of some key parameters on shear strength and softening behavior of lunar soil simulant can be easily obtained based on this constitutive model.

KEYWORDS

Lunar soil simulant, Constitutive model, Shear dilatancy, Softening, Residual deformation

INTRODUCTION

The lunar exploration project first requires studying the interaction between lunar probes and lunar soil, but there are very few real lunar soil samples, so only lunar soil simulant with similar properties (these similar properties include basic physical indicators, particle grading and distribution, as well as particle shape, etc.) can be used to replace real lunar soil [1-4]. The key challenges faced in this endeavor involve understanding the interaction mechanisms between the lunar drilling equipment and lunar soil under low-stress conditions, as well as the unique mechanical properties of lunar soil in low gravity environments [3-5]. To address these challenges effectively, a reasonable constitutive model is an essential approach to accurately describe the mechanical properties of lunar soil simulant, which will provide a significant reference value for lunar soil drilling and sampling, design of landers, rovers, and drilling equipment on the moon.

The success rate of lunar surface sampling primarily depends on the understanding the constitutive characteristics of lunar soil. In the past decade, some empirical constitutive models have been established based on data fitting from experimental tests and numerical simulations. For example,

Hasan and Alshibli [6] simulated the triaxial compression test of JSC-1A （the name of lunar soil simulant developed by Johnson Space Center）lunar soil simulant using a three-dimensional particle flow code (PFC3D). Based on the experimental data, they established an empirical constitutive model for the peak internal friction angle, residual friction angle, density, and average normal stress. Hicher and Chang [7] established a constitutive model considering the surface energy effects caused by static electric forces of lunar soil particles based on triaxial compression test data. They analyzed the influence of surface energy on the shear strength of lunar soil. Richard [8] used the Cambridge model to describe the constitutive behavior of lunar soil based on triaxial test data. By adjusting the friction angle, the fitted the modified Cambridge model's yield surface and critical state line suitable for lunar soil. Zou et al. [9] developed an internal stress model to investigate the bearing capacity and shear strength of lunar soil simulant. Hou et al. [10] and Jiang et al. [11] also proposed a novel contact model of lunar soil particles to investigate the main mechanical properties of lunar soil simulant, the results indicated that the lunar soil simulant under low gravity environment are different from those on the earth. Liu et al. [12] established a variable constitutive model based on discrete element simulations to study the shear strength and elastoplastic behavior of lunar soil simulant under loose and dense conditions. Furthermore, Liu et al. [13] further proposed an equivalent boundary method based on this constitutive model to effectively address the computational cost issue in discrete element simulations for lunar soil drilling and sampling. Schafer et al. [14] used an elastic-plastic constitutive model for dynamic behavior of lunar soil to study the sampling process under different surface gravity environments. Liang et al. [15] used ABAQUS finite element software based on Cap Drucker-Prager model to simulate the landing impact process of a lander. Mao and Liu [16] developed a smoothed particle hydrodynamics (SPH) model with the elastic-perfectly plastic constitutive equation and Drucker-Prager yield criterion to simulate the electrostatic transporting of multiple charged lunar dust particles. Li et al. [17] also developed a new wear mechanical model for lunar dust to investigate the mechanical properties of lunar dust (including adhesion, contact, and wear), and rationality of the model was verified through experiments. These models effectively reflect some special mechanical properties of lunar soil simulant from a certain perspective and obtain corresponding applications. However, there are few or almost no models consider strain softening characteristics caused by cementation failure in the lunar soil simulant, it is difficult to describe the shear dilatancy and softening characteristics of lunar soil simulant under low stress levels.

Focusing on this problem, many experimental and simulation works have shown that lunar soil simulant exhibits significant shear dilatancy and softening characteristics under low stress conditions [18-23]. A rational constitutive model should reflect the shear dilatancy and softening characteristics of lunar soil simulant under low stress levels. Though discrete element simulations can effectively capture microstructural deformation features and related mechanical properties, the small size of sample used in calculations cannot fully represent the macroscopic mechanical behavior of the entire material. Moreover, due to the lack of research on the shear dilatancy behavior of lunar soil simulant and strain softening caused by cementation failure at low stress levels, the understanding of the mechanisms of the shear dilatancy and softening remains unclear, resulting in lack of a clear understanding of mechanical properties of lunar soil in low gravity environment. Therefore, it is important to establish a

micromechanical constitutive model that considers the shear dilatancy and softening characteristics of lunar soil simulant. This would help reveal the constitutive properties of lunar soil in low gravity environment and accurately describe its mechanical behavior.

ELASTOPLASTIC CONSTITUTIVE THEORY

The schematic diagram of shear stress-shear strain curve is shown in Figure 1. This curve can be divided into three stages as the shear strain changes:

(1) Linear elastic stage: In this stage, the shear strain of the lunar soil simulant is relatively small, and the shear stress has not reached the yield threshold. The deformation of the lunar soil simulant sample can be considered as elastic.

(2) Elastoplastic stage: With increasing shear strain, the shear stress gradually reaches its peak value. Then, the sample enters the elastoplastic stage. At this time, the shear stress of the lunar soil simulant has reached the peak stress, the contact between particles begins to yield, and the shear stiffness decreases. In the process of shearing, there will also be relative deformation in the normal direction, and the sample will experience shear dilatancy.

(3) Softening stage: With the gradual increase of shear stress, the internal cementation of the lunar soil simulant is destroyed, and softening occurs, and the shear stress is greatly reduced. These three stages can be called elastic, elastoplastic, and softening stages, respectively (See Figure 1).

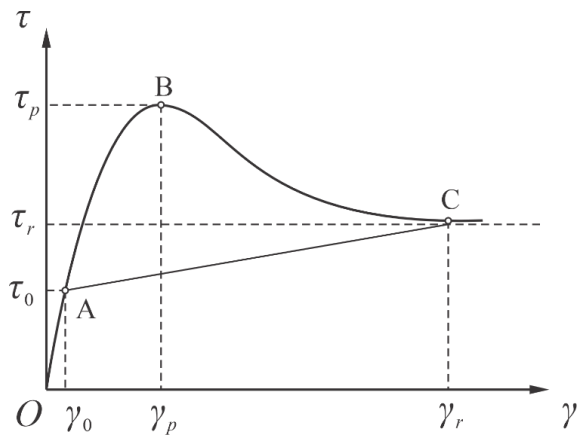

Fig.1 - Schematic diagram of shear stress-shear strain curve of lunar soil simulant

The current work will be based on the shear stress-shear strain curve OABC shown in Figure 1, which can be divided into two parts: the first part is the elastoplastic hardening stage OAC, and the second part is the shear dilatancy and softening stages ABC. Based on these two parts, corresponding constitutive equations will be proposed.

Development of the elastoplastic strain-hardening model

Based on the theory of elastoplasticity, during the process of shear deformation in the lunar

soil simulant specimen, the plastic potential function *Q*, the yield function *F*, the elastic scalar factor $d\lambda$, and the hardening modulus *H* are known. The strain increment of the lunar soil simulant under loading can be divided into two parts: elastic reversible and plastic irreversible strain increments:

$$d\varepsilon_i = d\varepsilon_i^e + d\varepsilon_i^p \quad (i = 1, 2)$$

(1)

In the equation, i =1, 2 correspond to the tangential direction and normal direction, respectively.

Furthermore, based on Hooke's Law, the relationship between the elastic deformation increment and the stress increment of the lunar soil simulant can be obtained:

$$d\sigma_i = K_{ij} d\varepsilon_j^e = K_{ij}(d\varepsilon_j - d\varepsilon_j^p)$$

(2)

where K_{ij} is the elastic stiffness matrix.

According to the plastic flow rule, the plastic strain increment of the lunar soil simulant can be obtained:

$$d\varepsilon_i^p = d\lambda \frac{\partial Q}{\partial \sigma_i} = \frac{1}{H}\left(\frac{\partial F}{\partial \sigma_j} d\sigma_j\right)\frac{\partial Q}{\partial \sigma_i} \tag{3}$$

Substituting (3) into (2) and multiplying both sides by $\frac{\partial F}{\partial \sigma_i}$, we obtain:

$$\frac{\partial F}{\partial \sigma_i} d\sigma_i = \frac{\frac{\partial F}{\partial \sigma_i} K_{ij} d\varepsilon_j}{1 + \frac{1}{H}\frac{\partial F}{\partial \sigma_k} K_{kl} \frac{\partial Q}{\partial \sigma_l}} \tag{4}$$

By substituting (4) into (3), the plastic strain increment can be obtained:

$$d\varepsilon_i^p = \frac{\frac{\partial F}{\partial \sigma_r} K_{rs} d\varepsilon_s \frac{\partial Q}{\partial \sigma_i}}{H + \frac{\partial F}{\partial \sigma_k} K_{kl} \frac{\partial F}{\partial \sigma_l}} \tag{5}$$

Finally, by substituting (5) into (2), the relationship between the stress increment and the strain increment can be obtained.

$$d\sigma_i = \left(K_{ij} - \frac{K_{ir}\frac{\partial Q}{\partial \sigma_r}\frac{\partial F}{\partial \sigma_s} K_{sj}}{H + \frac{\partial F}{\partial \sigma_r} K_{rs} \frac{\partial Q}{\partial \sigma_s}}\right) d\varepsilon_j = K_{ij}^{ep} d\varepsilon_j$$

(6)

Where K_{ij}^{ep} is the elastoplastic stiffness matrix. Equation (6) represents the general form of the elastoplastic constitutive equation under non-associated flow rule. The hardening modulus *H* has

different expressions for isotropic hardening, kinematic hardening, and other cases. Since the tangential stress and tangential displacement of the lunar soil simulant eventually approach a stable curve (residual stress tends to stabilize) under shear loading conditions, the strain-hardening model is used here to describe this deformation mechanism.

Under the kinematic hardening model assumption, the initial yield function is assumed to be the Mohr-Coulomb yield function [20-24]:

$$F(\sigma_i) = \tau - \sigma_n \tan(\varphi_b) - c \tag{7}$$

In the equation, c represents the cohesive strength of the cementation of the lunar soil simulant.
The subsequent yield surface of the kinematic hardening model in stress space is obtained by rigid translation. Therefore, the subsequent yield function can be assumed as:

$$f(\sigma_i, \varepsilon_i^p, k) = F(\sigma_i - \alpha_i) - k \tag{8}$$

In the equation, ε_i^p is the plastic strain, α_i is the back stress, which is a function of the coordinates of the loading surface center and the plastic strain. *k* is the hardening parameter.

In plastic deformation, the yield function satisfies the consistency condition:

$$df = \frac{\partial F}{\partial \sigma_i} d\sigma_i - \frac{\partial F}{\partial \sigma_i} \frac{\partial \alpha_i}{\partial \varepsilon_j^p} d\varepsilon_j^p = 0 \tag{9}$$

Based on the associative flow rule, by substituting (3) into (9), we obtain:

$$H = \frac{\partial F}{\partial \sigma_i} \frac{\partial \alpha_i}{\partial \varepsilon_j^p} \frac{\partial F}{\partial \sigma_j} \tag{10}$$

Assuming $d\alpha_i$ and $d\varepsilon_i^p$ are linearly relation, that is, following the Prager hardening rule:

$$d\alpha_i = c d\varepsilon_i^p \tag{11}$$

where *c* represents the work hardening function, which is expressed as follows:

$$c = \frac{\tau_r - \tau_0}{\gamma_r - \gamma_0} \frac{1}{\frac{\partial F}{\partial \sigma_i} \frac{\partial F}{\partial \sigma_j}} \tag{12}$$

In equation (12), τ_r represents the residual shear stress, and γ_r represents the residual shear strain. Substituting (11) into (10), we obtain:

$$H = c \frac{\partial F}{\partial \sigma_i} \frac{\partial F}{\partial \sigma_j} \tag{13}$$

By combining (6), (12), and (13), the incremental stress-strain constitutive equation for the kinematic hardening model can be respectively obtained as follows:

$$d\tau = (K_{ss} - \frac{K_{ss}K_{ss}}{A}) d\gamma - \frac{\mu K_{nn} K_{ss}}{A} d\varepsilon, \quad d\sigma = -\frac{\mu K_{nn} K_{ss}}{A} d\gamma + (K_{nn} - \frac{\mu K_{nn} K_{nn} \mu}{A}) d\varepsilon \tag{14}$$

In the equation (14), $A = \mu K_{nn} \mu + K_{ss} + \frac{\tau_r - \tau_0}{\gamma_r - \gamma_0}$.

Usually, the normal stress is a constant value, and its stress increment $d\sigma = 0$. Therefore, we have:

$$d\tau = \frac{\tau_r - \tau_0}{\gamma_r - \gamma_0 + \frac{\tau_r - \tau_0}{K_{ss}}} d\gamma \tag{15}$$

Equation (15) reflects the deformation characteristics of the lunar soil simulant under shear loading. In Figure 1, the strengthening segment passes through the initial yield point A (γ_0, τ_0) and the residual strength point C (γ_r, τ_r). Thus, from equation (15), the following is obtained:

$$\tau_f = \frac{\tau_r - \tau_0}{\gamma_r - \gamma_0 + \frac{\gamma_r - \gamma_0}{K_{ss}}} (\gamma - \gamma_0) + \tau_0 \tag{16}$$

Since K_{ss} is much larger than $\tau_r - \tau_0$, the $\frac{\tau_r - \tau_0}{K_{ss}}$ in equation (16) can be neglected, that is:

$$\tau_f = \frac{\tau_r - \tau_0}{\gamma_r - \gamma_0} (\gamma - \gamma_0) + \tau_0 \tag{17}$$

In the initial elastic segment OA of Figure 1, $\tau_{OA} = K_{si} \gamma$ (18)

In the equation (18), K_{si} is the initial shear stiffness.

Development of the shear dilatancy and softening model

Due to the cementitious particles and their irregular geometrical shape in the real lunar soil [1], as shown in Figure 2, during the shear process, the cementitious particles in the lunar soil and their micro-asperities interlock with each other, leading to an enhanced stress concentration effect and the formation of shear planes that are prone to being sheared. This shearing action causes damage to the particles of lunar soil simulant. When the shearing of micro-asperities accumulates to a certain extent, the intact regions undergo instantaneous failure, resulting in a sudden drop in stress, known as the softening phenomenon. In most cases, as the particles undergo shear deformation, the shear stress first undergoes an increasing stage and then experiences a significant decrease, exhibiting both hardening and softening phenomena.

The shear dilatancy of lunar soil simulant primarily arises from the irregular surface morphology of its structural planes. It reflects the complex relationship between the tangential and normal deformations of the lunar soil simulant, and affects the variation of stress during tangential deformation. When subjected to shear, the interlocking action between micro-asperities inside the cementitious

particles significantly increases stress concentration. The appearance of sheared contact surfaces reduces the shear dilatancy angle. Therefore, the lunar soil simulant exhibits both shear dilatancy and softening during deformation. As deformation and damage of the cementitious material accumulate, it causes macroscopic structural failure of the cementitious material and significantly reduces stress, which is known as softening phenomenon. During the loading process, the shear stress of the lunar soil simulant first rises and then experiences a sharp drop, corresponding to the phenomena of shear dilatancy and softening, respectively.

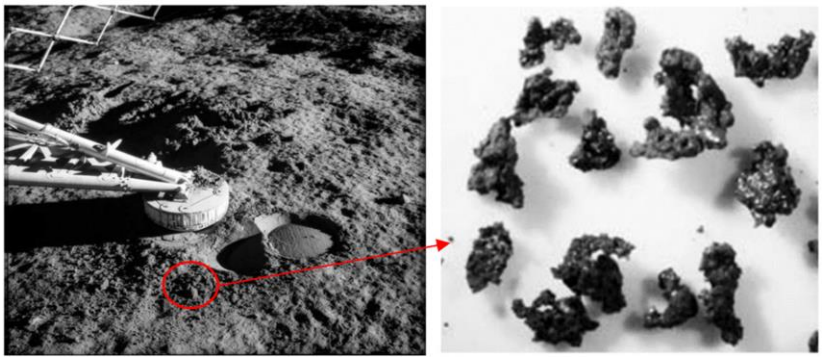

Fig.2 – Lunar soil and cementitious particles in the lunar soil [1].

The shear dilatancy and softening phenomena proposed in the present work are mechanical characteristic that lunar soil simulant during shear deformation process, and in our previous numerical simulations also focused on describing this deformation characteristic [21-23]. Based on this characteristic, we can assume an initial shear stress that represents the occurrence of both shear dilatancy and softening in the vertical direction when the lunar soil simulant undergoes shear deformation, with the softening phenomenon resulting from the failure of the cementitious materials. By isolating the strengthening mechanism, this part is considered the first component of the constitutive model for the lunar soil simulant. Combining the aforementioned the shear dilatancy-softening rules and previous studies [24-28], the following formula can be proposed to represent the shear dilatancy and softening characteristics of lunar soil simulant:

$$\tau(\gamma)=\frac{a(\gamma-\gamma_0)}{1+c(\gamma-\gamma_0)^{k_1}} \tag{19}$$

In the formula, *a*, *c* are parameters; k_1 is an amplitude parameter that can adjust the magnitude of the post-peak softening for different lunar soil simulants; γ_0 represents the initial yielding strain. The advantages of this formula mainly include three aspects: it has only one extremum within the specified region; the slope of the function tangent line at the peak is 0; as the strain approaches infinity, the function approaches 0. The function should also satisfy passing through point $P(\gamma_p, \tau p-\tau f(\gamma_p))$, which can be simplified as passing through point (γ_p, τ_0). $\tau f(\gamma_p)$ represents the shear strength of the follow-up strengthening model at γ_p. From this, we can obtain:

$$a = \frac{k_1(\tau_p - \tau_0)}{(k_1 - 1)(\gamma_p - \gamma_0)}, \quad c = \frac{1}{(k_1 - 1)(\gamma_p - \gamma_0)^{k_1}} \tag{20}$$

Substituting (20) into (19), we obtain:

$$\tau(\gamma) = \frac{k_1(\tau_p - \tau_0)(\frac{\gamma - \gamma_0}{\gamma_p - \gamma_0})}{k_1 - 1 + (\frac{\gamma - \gamma_0}{\gamma_p - \gamma_0})^{k_1}} \tag{21}$$

Furthermore, considering that the magnitude of shear stress in lunar soil simulant is also related to the normal stress, the compressive strength of cementitious material, and other factors, by modifying the above formula based on these two factors, a more comprehensive formula for the initial shear stress t_j can be obtained:

$$\tau_j = \frac{k_1(\tau_p - \tau_0)(\frac{\gamma - \gamma_0}{\gamma_p - \gamma_0})(1 - \frac{\sigma_n}{\sigma_t})}{k_1 - 1 + (\frac{\gamma - \gamma_0}{\gamma_p - \gamma_0})^{k_1}} \tag{22}$$

In the above formula, τ_{p} represents the peak shear stress, τ_0 represents the initial yield stress, σ_{t} represents the uniaxial compressive strength, which is approximately the compressive strength of the entire lunar soil simulant, and σ_{n} represents the normal stress on the lunar soil simulant during loading.

Establishment of the constitutive model and determination of model parameters

Based on the above analysis, the constitutive relationship for the lunar soil simulant in this study can be expressed as follows:

$$\tau = \begin{cases} \tau_{OA} & (\gamma \in (0 \quad \gamma_0)) \\ \tau_f + \tau_j & (\gamma \in (\gamma_0 \quad \gamma_r)) \end{cases} \tag{23}$$

After determining the constitutive model, the next step is to further determine the parameters in the constitutive model. The meanings and determination methods of the parameters are as follows:

(1) Peak shear strain ε_{p}, residual shear strain ε_{r}, basic friction angle φ_{b}, and residual friction angle φ_{r} can all be obtained from the monotonic shear loading tests.

(2) Peak shear stress τ_{p}: The peak shear stress of the lunar soil simulant can be obtained using the empirical equation proposed by Barton and Choubey [29], which is given by:

$$\tau_p = \sigma_n \tan\left[C \log\left(\frac{\sigma_{CS}}{\sigma_n}\right) + \varphi_b\right] \tag{24}$$

where *C* represents the strength of the cohesive force between the bonding particles, σ_{CS} represents the compressive strength of the cementitious material in lunar soil simulant.

(3) The residual shear stress τ_r is determined by Coulomb's criterion:

$$\tau_r = \sigma_n \tan \varphi_r \tag{25}$$

(4) Initial normal stiffness K_{ni}: Obtained from the normal monotonic loading test, its value is the initial slope of the normal stress-normal strain curve, as shown in Figure 3(a). The initial shear stiffness K_{si} is obtained from direct shear cyclic tests, and its value is related to the normal stress. Based on the shear stress-shear strain curve, the slope of the unloading portion after exceeding the initial yield point represents the initial shear stiffness, as shown in Figure 3(b). When it is challenging to determine through experiments, Bandis et al. [30] proposed an empirical formula for the initial shear stiffness K_{si} based on a large number of tests:

$$K_{si} = K_j(\sigma_n)^{n_j} \tag{26}$$

Where K_j is the stiffness coefficient, σ_n is the normal stress, and n_j is the initial stiffness exponent.

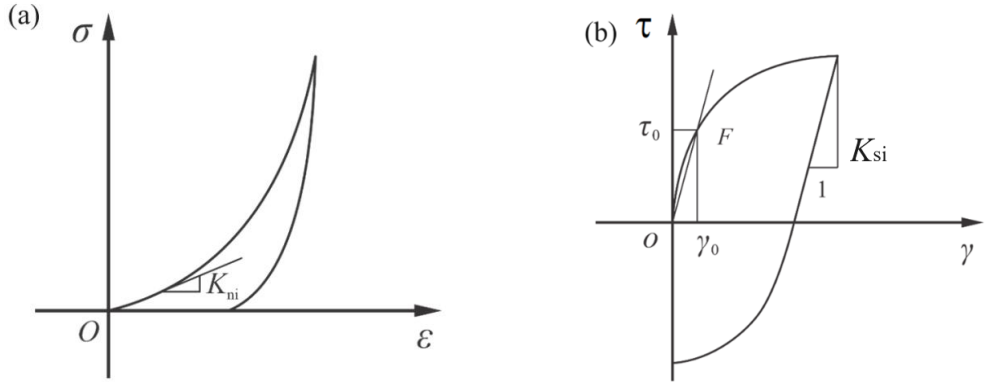

Fig.3 - Diagrams of (a) normal stress-normal strain curve and (b) shear stress-shear strain curve.

(5) The initial yield stress τ_o and the initial yield strain γ_0: Based on the method shown in Figure 3(b) for determining the initial shear stiffness, draw a line with a slope of K_{si} from the origin *o* which intersects the shear stress-shear strain curve at point *F*. This point *F* represents the initial yield point. When it is difficult to determine the initial yield point, according to Goodman's experimental tests [31], the initial yield point in the elastic phase is generally located at around 70% to 90% of the peak shear strength. Considering the yield characteristics of lunar soil simulant, we can estimate the initial yield point by taking 70% of the peak shear strength [20].

(6) The amplitude parameter k_1 reflects the shear dilatancy and softening characteristics of the material, which is related to the magnitude of the normal stress, and the adhesive force between cementing particles. Typically, for relatively rough particles of lunar soil simulant, the value of k_1 is taken as 4, which can be obtained from the first cycle of the shear loading test curve.

DIRECT SHEAR RESULTS AND VALIDATION OF THE MODEL

Based on the above derived constitutive model and the determined parameters, direct shear test and model validation will be conducted using this constitutive model. The parameters involved in the constitutive model are listed in Table 1.

Tab.1 - Key parameters of the model

γ_p (%)	φ_b /(°)	σ_{cs}/kPa	σ_τ/kPa	k_1
2.65	40	1000	700	4
γ_f (%)	φ_r /(°)	*C*/ kPa	γ_0 (%)	
8	30	4	1.35	

Figure 4(a) shows the shear stress-shear strain curves obtained by this theoretical constitutive model under different low normal stresses. From Figure 4(a), it can be observed that the shear stress first reaches its peak value, then rapidly decreases until it enters a relatively stable residual deformation stage, reflecting the shear dilatancy and softening characteristics of the lunar soil simulant. The peak shear stress and residual shear stress increase with the increase of the normal stress. Based on the shear stress-shear strain curves in Figure 4(a), the shear strength τ_p can be obtain under different normal stresses, as shown in Figure 4(b). By comparing with previous experimental results and theoretical results, there is a good agreement with experimental tests of Zhang et al. [18], indicating that the model not only captures the shear dilatancy and softening characteristics of the lunar soil simulant but also successfully simulates the direct shear test. Moreover, the values of cohesive force *C* and basic internal friction angle φ_b in the theoretical model are 4 kPa and 40^0, respectively. When the porosity e=1, the values *C* and φ_b in the experiment tests are 4 and 40.35^0 respectively. These two parameters used in constitutive model are almost consistent with those obtained in the experiment, and all belong to the range of variation of real lunar soil [1, 32], which further validates the rationality of the proposed model in the present work.

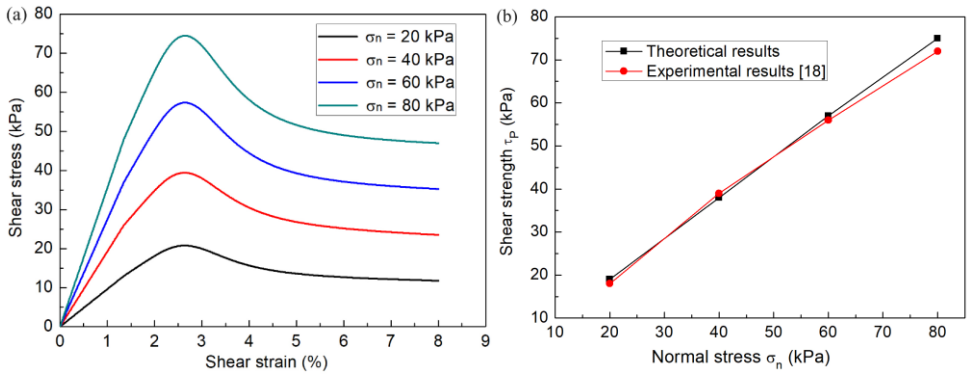

Fig.4 - Direct shear results at different normal stresses: (a) shear stress-shear strain curves, and (b) Comparison of shear strength obtained from experiments and theoretical model.

INFLUENCES ANALYSIS OF MODEL PARAMETERS

Since k_1 is an amplitude parameter that can adjust the magnitude of the post-peak softening of lunar soil simulant, the change in k_1 value will affect the residual shear stress after softening. Figure 5 shows the shear stress-shear strain curves at various amplitude parameters. It is found that the change in k_1 hardly affects the magnitude of peak shear stress, but it has a significant impact on the softening behavior and the magnitude of residual shear stress. When k_1=2 and 3, after the sample reaches their peak shear stress, although there is softening, the softening phenomenon is not obvious and there is no relatively stable residual deformation stage. The degree of softening increases as the value of k_1 increases, when k_1=4, there is a noticeable softening phenomenon, and relatively stable residual shear stress is observed, which is suitable for the shear deformation characteristics of lunar soil simulant. Therefore, k_1 = 4 is used in the present study.

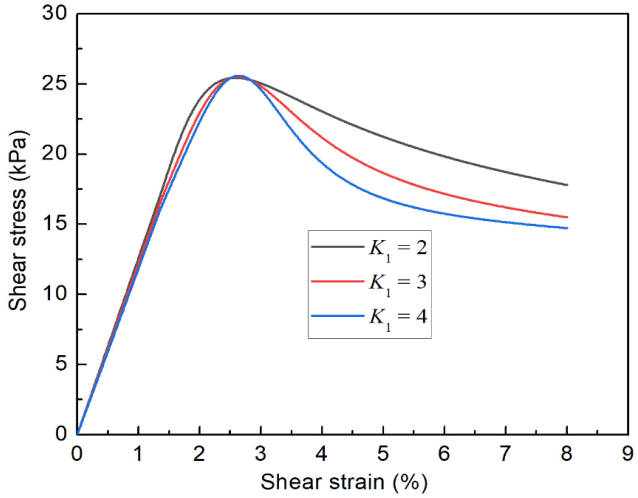

Fig.5 - Shear stress-shear strain curves at various amplitude parameters (K_1)

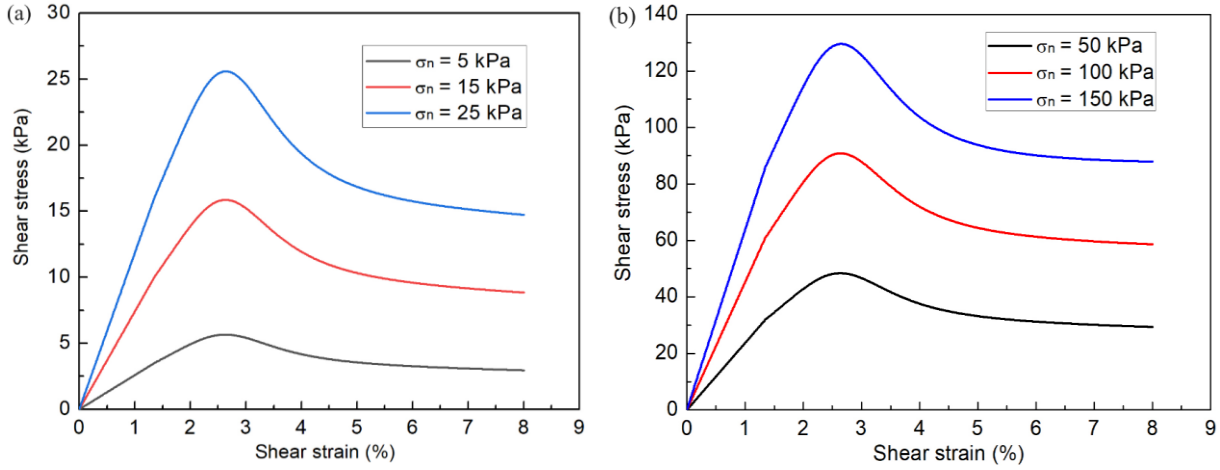

Fig.6 - Shear stress-shear strain curves of lunar soil simulant specimens under different normal stress conditions: (a) low normal stress, and (b) conventional normal stress.

Figure 6(a) and (b) show the shear stress-shear strain curves of the lunar soil simulant samples under low normal stress and conventional normal stress conditions, respectively. From Figure 6, it can be observed that the shear stress first increases to its maximum value and then softens, leading to a rapid decrease in shear stress and entering the residual shear stress stage. It indicates that lunar soil simulant exhibits significant shear dilatancy and softening characteristics both at low and conventional normal stress conditions. Moreover, at low normal stress, as the normal stress increases, the peak shear stress and residual stress increase. Similarly, at conventional normal stress, with an increase in the normal stress, the peak shear stress and residual stress also increase.

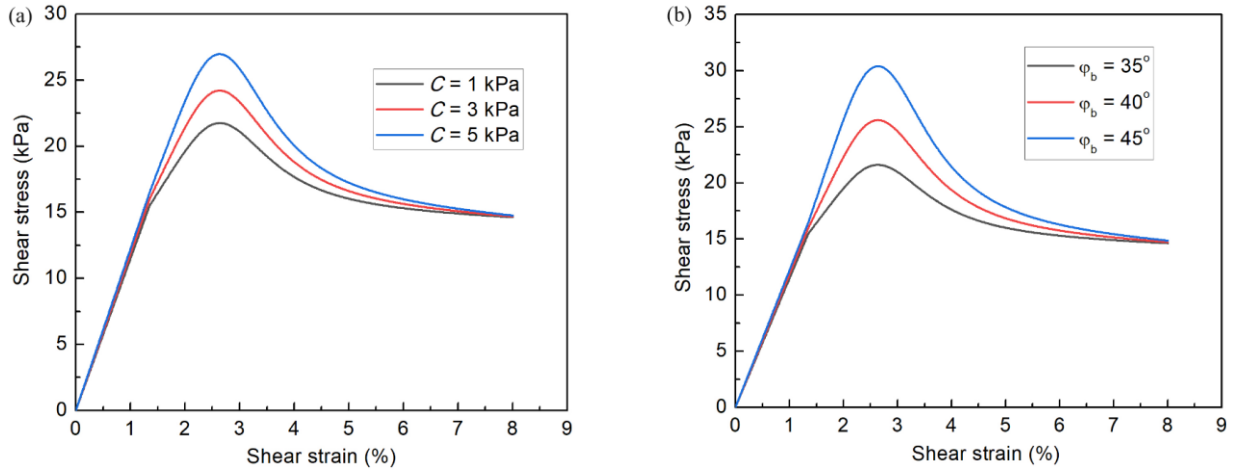

(a) *(b)*

Fig.7 - Influences of simulation parameters on the stress-shear strain curves of lunar soil simulant specimens.

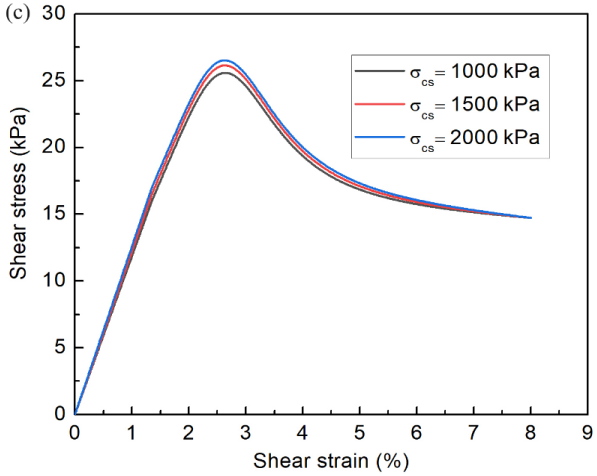

Fig.7 - Influences of simulation parameters on the stress-shear strain curves of lunar soil simulant specimens. (a) different particle cohesions, (b) different internal friction angles, and (c) different compressive strengths of cementitious particles.

To further reflect the influences of model parameters on the stress-strain curves and the shear

dilatancy and softening characteristics of lunar soil simulant specimens, Figure 7 presents the stress-shear strain curves under different values of particle cohesion, particle internal friction angle, and compressive strength of the cementitious material in lunar soil simulant. From Figure 7, it can be observed that regardless of how the model parameters are changed, the overall curve patterns remain unchanged, namely, the shear stress first increases to reach the peak stress, followed by softening and eventually reaching a stable residual stress stage. This trend also reflects the pronounced shear dilatancy and softening characteristics of the lunar soil simulant. In Figure 7(a), as the particle cohesion increases, the peak stress increases, and the residual stress after softening also increases. Finally, with increasing shear strain, the residual stress tends to stabilize. Similarly, for different variations in the particle internal friction angle (Figure 7(b)) and the compressive strength of the cementitious material in lunar soil simulant (Figure 7(c)), a similar trend is observed, with higher values resulting in increased peak stress and residual stress. Compared to the internal friction angle and particle cohesion, the influence of change in compressive strength of cementitious material on shear strength is very small.

CONCLUSIONS

(1) In this study, an elastoplastic constitutive model is developed to effectively captures the shear dilatancy and softening characteristics of lunar soil simulant. The model uses the kinematic hardening equations based on the classical elastoplastic theory to describe this strengthening phenomenon, and reflects the softening characteristics by introducing the concept of initial shear stress, which effectively compensates for the shortcomings of existing constitutive models in the literatures.

(2) The model only requires fewer parameters to be determined, and all of which can be obtained through simple initial loading curves from direct shear tests.

(3) The model allows for the analysis of the influences of parameters such as normal stress, particle cohesion, internal friction angle, amplitude parameter, and compressive strengths of cementitious material on the peak strength, residual strength, shear dilatancy and softening characteristics of lunar soil simulant. These results will provide some references for a deeper understanding of the mechanical behavior of lunar soil and the mechanical analysis involved in lunar soil mining and future lunar base construction.

The model proposed in this study mainly focuses on dry lunar soil simulant. For the icy lunar soil in the south pole region of the moon, its deformation characteristics are different due to the special properties such as water content and ice soil cement, and the corresponding constitutive model also needs further research.

ACKNOWLEDGEMENTS

The authors acknowledge the financial support provided by the National Natural Science Foundation of China (Grant No. 52009097), Education Department of Hubei Province of China (Grant No. B2021080), and Natural Science Foundation of Wuhan Institute of Technology (Grant No. K2021035).

REFERENCES

[1] Carrier W D, Olhoeft G R, Mendell W., 1991. Physical properties of the lunar surface: Lunar Source Book, (Cambridge University Press) 475–594.
[2] Sun X M, Zhang R, Li X J, Zou M, Wang C, ChenL., 2022. JLU-H: A novel lunar highland regolith simulant for use in large-scale engineering experiments. Planetary and Space Science, vol. 221: 105562. doi:10.1016/j.pss.2022.105562.
[3] Mills J N, Katzarova M, Wagner N J., 2022. Comparison of lunar and Martian regolith simulant-based geopolymer cements formed by alkali-activation for in-situ resource utilization. Advances in Space Research, vol. 69: 761–777. doi:10.1016/j.asr.2021.10.045.
[4] Dewoolkar M M, Edwards M, Walsh D., 2018. Shear strength and stiffness characterization of lunar simulant GRC-3. Journal of Aerospace Engineering, vol. 31: 04018024. doi:10.1061/(ASCE)AS.1943-5525.0000848.
[5] Yu H, Hu Z., 2013. Mechanical characteristics of a lunar regolith simulant at low confining pressure. Environmental Earth Sciences, vol. 71: 3697–3703. doi:10.1007/s12665-013-2763-7.
[6] Hasan A, Alshibli K A., 2010. Discrete element modeling of strength properties of Johnson Space Center (JSC-1 A) lunar regolith simulant. Journal of Aerospace Engineering, vol. 23: 157–165. doi:10.1061/(ASCE)AS.1943-5525.0000020.
[7] Hicher P Y, Chang C S., 2008. A constitutive model for lunar soil. 11th Biennial ASCE Aerospace Division International Conference on Engineering, Science, Construction, and Operations in Challenging Environments. doi:10.1061/40988(323)16.
[8] Richard A S., 2006. Cam cap models for lunar soil: a first look. Tenth Biennial ASCE Aerospace Division International Conference on Engineering, Construction, and Operations in Challenging Environments, Houston, Texas. doi:10.1061/40830(188)37.
[9] Zou M, Fan S C, Shi R Y, Yang Y J, Li J Q., 2015. Effect of gravity on the mechanical properties of lunar regolith tested using a low gravity simulation device. Journal of Terramechanics, vol. 60: 11–22. doi:10.1016/j.jterra.2015.04.003.
[10] Hou X Y, Ding T X, Chen T, Liu Y M, Li M, Deng Z Q., 2019. Constitutive properties of irregularly shaped lunar soil simulant particles. Powder Technology, vol. 346: 137–149. doi:10.1016/j.powtec.2019.02.012.
[11] Jiang M J, Shen Z F, Thornton C., 2013. Microscopic contant model of lunar regolith for high efficiency discrete element analysises. Computers and Geotechnics, vol. 54: 104–116. doi:10.1016/j.compgeo.2013.07.006.
[12] Liu T X, Liang L, Zhao Y, Cao D Q., 2020. An alterable constitutive law of high-accuracy DEM model of lunar soil. Advances in Space Research, vol. 66: 1286–1302. doi:10.1016/j.asr.2020.06.026.
[13] Liu T X, Liang L, Zhao Y, Cao D Q., 2020. Equivalent boundary model of lunar soil drilling simulation by DEM. Journal of Terramechanics, vol. 91: 85–95. doi:10.1016/j.jterra.2020.06.003.
[14] Schafer C M, Scherrer S, Buchwald R, Maindl T I, Speith R, Kley W., 2017. Numerical simulations of regolith sampling processes. Planetary and Space Science, vol. 141: 35-44. doi:10.1016/j.pss.2017.04.015.
[15] Liang D P, Chai H Y., 2012. Lunar soil constitutive model and finite element modeling for landing impact simulation. Spacecraft Engineering, vol. 21: 18–24. doi:10.1016/j.jrmge.2023.04.025.
[16] Mao Z R, Liu G R., 2018. A smoothed particle hydrodynamics model for electrostatic transport of charged lunar dust on the moon surface.Computational Particle Mechanics, vol. 5: 539-551. doi:10.1007/s40571-018-0189-4.
[17] Li R J, Cui Y H, Feng Y L, Wang J S, Huang W, Sui Y, Ren D P., 2023. New mechanical models to study the impact of contact, wear, and adhesion of lunar dust on space materials. International Journal of Applied Mechanics, vol. 15. doi:10.1142/S1758825123500254.
[18] Zhang Y, Chen S X, Yu F, Li J, Gao H., 2015. Experimental study of mechanical properties of lunar soil simulant CAS-1 under low stress. Chinese Journal of Rock Mechanics and Engineering, vol. 34: 174–181. doi:10.13722/j.cnki.jrme.2015.01.019.
[19] Jiang M J, Yin Z Y, Shen Z F., 2016. Shear band formation in lunar regolith by discrete element analyses. Journal of Granular Matter, vol. 18: 1–14. doi:10.1007/s10035-016-0635-z.
[20] Zou W L, Li Y L, Chen L, Zhang J F, Wang X Q., 2016. Mechanical properties of QH-E lunar soil simulant at low confining stresses. Journal of Aerospace Engineering, vol. 29: 04015036. doi:10.1061/(ASCE)AS.1943-5525.0000526.
[21] Li Y L, Zou W L, Wu W P, Chen L., 2018. Discrete element modeling of strength properties and failure modes of QH-E lunar soil simulant at low confining stresses. Stavební obzor-Civil Engineering Journal, vol. 2: 211–

226. doi:10.14311/CEJ.2018.02.0017.
[22] Li Y L, Zou W L, Wu W P, Chen L, Chu X H., 2018. Triaxial compression tests of QH-E lunar soil simulant under constant mean principal stress path using discrete element method simulations. Granular matter, vol. 20: 79. doi:10.1007/s10035-018-0855-5.
[23] Li Y L, Wu W P, Chu X H, Zou W L., 2020. Effects of stress paths on triaxial compression mechanical properties of QH-E lunar soil simulant by DEM simulation. Granular matter, vol. 22: 32. doi:10.1007/s10035-020-0999-y.
[24] Plesha M E., 1987. Constitutive models for rock discontinuities with dilatancy and surface degradation. International Journal of Numerical and Analytical Methods in Geomechanics, vol. 11: 345–362. doi:10.1002/nag.1610110404.
[25] Desai C S, Fishman K L., 1991. Plasticity-based constitutive model with associated testing for joints. International Journal of Rock Mechanics and Mining Sciences & Geomechnics Abstracts, vol. 28: 15–26. doi:10.1016/0148-9062(91)93229-Y.
[26] Wang J G, Ichikawa Y, Leung C F., 2003. A constitutive model for rock interfaces and joints. International Journal of Rock Mechanics and Mining Sciences, vol. 40: 41–53. doi:10.1016/S1365-1609(02)00113-2.
[27] Cai M, Horii H., 1992. A constitutive model of highly jointed rock masses. Mechanics of Materials, vol. 13: 217–246. doi:10.1016/0167-6636(92)90004-W.
[28] Xiao W G, Dui G S, Chen T L, Ren Q W., 2009. A study of constitutive model coupling dilatancy and degradation for jointed rock. Chinese Journal of Rock Mechanics and Engineering, vol. 28: 2535–2543. doi:10.1016/S1874-8651(10)60073-7.
[29] Barton N, Choubey V., 1977. The shear strength of rock joints in theory and practice. Rock Mechanics and Rock Engineering, vol. 10: 1–54. doi:10.1007/BF01261801.
[30] Bandis S C, Lumden A C, Barton N R., 1983. Fundamentals of rock joint deformation. International Journal of Rock Mechanics and Mining Sciences and Geomechanics Abstracts, vol. 20: 249–268. doi:10.1016/0148-9062(83)90595-8.
[31] Goodman R E., 1974. The mechanical property of joints. Proceedings of the 3rd Cong ISRM(Part A). 127–140. doi:10.1016/0148-9062(75)90743-3.
[32] Slyuta E N., 2014. Physical and mechanical properties of the lunar soil (a review). Solar System Research, vol. 48: 330-353. doi:10.1134/s0038094614050050.